JOURNAL OF MATERIALS SCIENCE 28 (1993) 4092–4098

Strain-dependent behaviour of microporous polyethylene with a negative Poisson's ratio

K. L. ALDERSON, K. E. EVANS
Department of Materials Science and Engineering, The University of Liverpool, P.O. Box 147, Liverpool L69 3BX, UK

Recent papers have discussed particular forms of expanded polytetrafluoroethylene (PTFE) and ultra-high molecular weight polyethylene (UHMWPE) that exhibit large negative Poisson's ratios due to their complex microstructures. These consist of an open network of nodules interconnected by fibrils. Two geometric models have been developed to explain the effect in PTFE; one based on nodule translation and the other on nodule rotation. Data are presented for the strain-dependent variation of the Poisson's ratio of UHMWPE under compression and the models are applied. The translation model alone accurately describes the variations in Poisson's ratio as a function of compressive strain.

1. Introduction

In the last five years, a number of synthetic materials have been produced that demonstrate a negative Poisson's ratio [1–6]. Such materials expand both transversely to and along the direction of an applied load. Such materials (referred to as auxetic materials) have been fabricated from foams [1, 2], microporous polymers [3–5] and polymer gels [6]. Molecular structures have also been suggested that would demonstrate such an effect [7]. The advantages of auxetic materials have been discussed [1, 8, 9] and include improved shear moduli, indentation resistance and plane strain fracture toughness.

The first example of an auxetic microporous polymer identified was a form of expanded polytetrafluoroethylene (PTFE) [3]. The microstructure of this material comprises an interconnecting network of nodules and fibrils whose cooperative interaction under an applied load produces the negative Poisson's ratio, ν [3, 4]. Two simple geometric models have been developed [10] that predict ν for the material in terms of simple geometric parameters of the microstructure. This consists of elliptically shaped nodules interconnected by fibrils. It was found that both models proposed were required to characterize the tensile strain dependence of ν for the PTFE. The first model is a transverse translation model and it describes movement of the nodules caused by the fibrils becoming taut, producing a lateral expansion. The second model is a rotation model and this describes the rotation of the nodules producing further lateral expansion. These changes in microstructure are illustrated in Fig. 1 and were confirmed by SEM examination [3].

More recently, a similar microstructure has been fabricated using ultra-high molecular weight polyethylene (UHMWPE) and negative ν values were again observed [5]. Qualitatively, the microstructures are similar but significant differences do exist. In this paper, detailed results for the variation of ν as a function of compressive strain are presented for auxetic, microporous UHMWPE. The earlier geometric model [10] is then adapted to compression testing to try to describe this effect.

2. Experimental procedure

2.1. Fabrication route

In order to fabricate UHMWPE with a negative ν, a novel thermoforming processing route has been developed [11] consisting of three distinct stages: compaction, sintering, and extrusion. Full details of this processing route are to be found in a previous paper [5], but, for completeness, a summary of the procedures are given here.

Two grades of UHMWPE powder were used (GUR 415 and GUR 412, Hoechst, Hounslow, UK) and the entire process took place in a specially designed extrusion rig. The extruder was first fitted with a blanked off die and heated to 110 °C. The barrel was then filled with UHMWPE powder and the entire system allowed to reach equilibrium. After 10 min, the plunger of the extruder was driven into the barrel by a Schenk mechanical testing machine at a rate of 20 mm min^{-1} until a pressure of 0.04 GPa was reached. This pressure was maintained for 20 min, resulting in a well-compacted rod.

The compacted rod was then sintered at a temperature of 160 °C for 20 min before the extruder plunger was driven into the barrel at a rate of 500 mm min^{-1}, forcing the material through a 5 mm diameter die.

Initial work was carried out using an extruder barrel of diameter 15 mm. The extrudate expanded to a diameter of 10 mm but had partial cup-and-cone fractures at regular intervals along its length. In an attempt to obtain a more consistent material whilst retaining the required negative Poisson's ratio, the diameter of the extruder barrel was reduced from

0022–2461

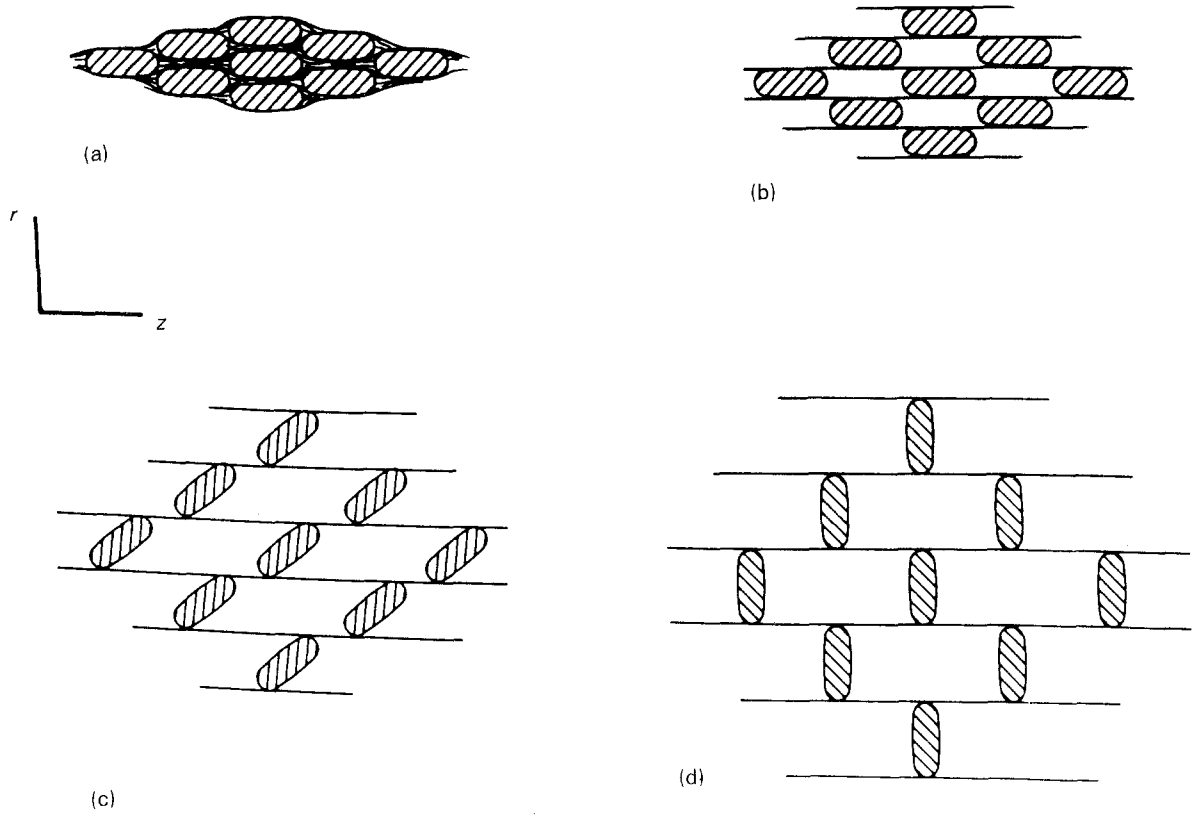

Figure 1 A schematic representation of the structural changes observed in microporous PTFE undergoing tensile loading in the z direction: (a) fully densified microstructure, (b) fibrils in tension causing a lateral expansion due to the movement of the nodules, (c) further lateral expansion due to the rotation of the nodules, and (d) fully expanded microstructure. Note that only a small proportion of fibrils have been included for clarity.

15 mm to 10 mm whilst all other processing conditions were maintained. The extrudate consisted of smooth, continuous material with cup-and-cone fractures restricted to the specimen ends. Again, the material expanded to a diameter of about 9 mm.

2.2. Measurement of ν

Owing to the small size of the specimens generated, it was not possible to measure strains (and thus obtain Poisson's ratio values) using standard tensile testing methods. Instead, the specimens were subjected to compression testing in the radial direction and the strains in the material measured using a simple photographic technique. From these measurements, a single ν for each section of the extrudate can be obtained from

$$\nu_{rz} = -\frac{\varepsilon_z}{\varepsilon_r} \quad (1)$$

where the load is applied in the r direction, with the r and z directions being defined in Fig. 2.

2.3. Microscopic examination of the UHMWPE

Samples of the material were taken from both types of extrudate and were mounted on aluminium stubs. These were then gold-coated using a sputter coater and observed in an SEM at magnifications of up to × 1250.

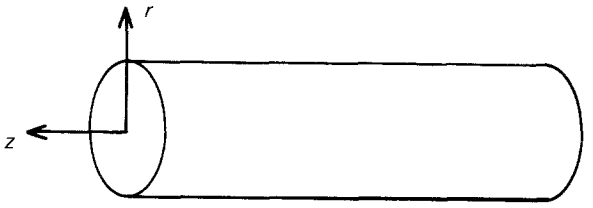

Figure 2 Schematic drawing showing the axis system used in the compression testing.

3. Translation and rotation network models

Full details of the two geometric tensile models developed for PTFE can be found in previous papers [4, 10]. However, these equations cannot be applied directly to compression testing. For this case, it is necessary to derive a revised set of equations and the derivations based on geometry are given below. It should be noted that both these simple models are two-dimensional but because the UHMWPE specimens are axisymetric, two-dimensional models are sufficient to describe experimental behaviour. It should also be noted that, in the case of UHMWPE, the fibrils are oriented in the radial or r direction, whereas, for PTFE, the fibrils are aligned in the axial direction.

Fig. 3 is a schematic representation of the translation (Fig. 3a) and the rotation (Fig. 3b) models, with a and b being the major and minor lengths of a set of rectangular particles interconnected by an array of

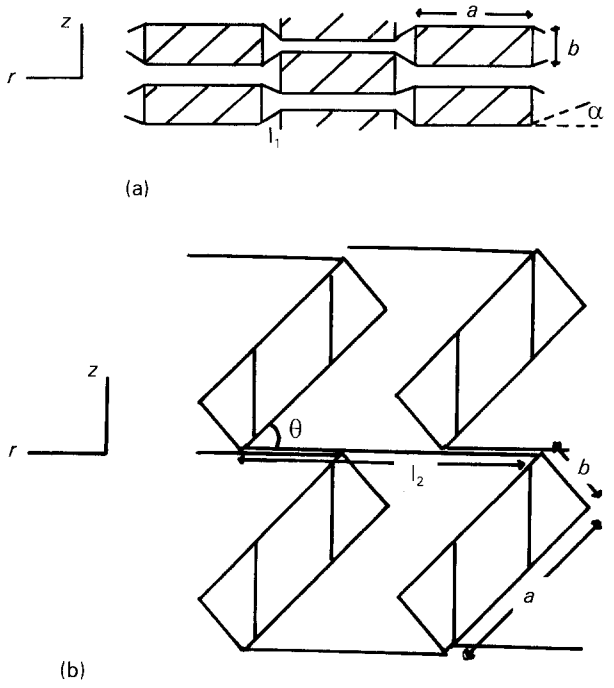

Figure 3 Schematic representation of the two geometric models: (a) for translation due to the movement of the particles as the fibrils become relaxed, and (b) for rotation due to the rotation of the particles.

inextensible rods of length l_1 for the translation model and length l_2 for the rotation model. For simplicity, a rectangular array is assumed and in both cases, a compressive strain in the r direction results in a contraction in the z direction, leading to a negative ν_{rz}.

It is possible for both models to calculate ν_{rz} as a function of geometry. Considering firstly the translation model, from Fig. 3 we may consider a space-filling unit cell of sides

$$r = 2a + 2l_1\cos\alpha \tag{2}$$

$$z = 2b - 2l_1\sin\alpha \tag{3}$$

where α is the angle between the rod and the r axis. Now, from Equation 1 and by definition

$$\nu_{rz} = -\frac{\varepsilon_z}{\varepsilon_r} = -\frac{(\Delta z/z)}{(\Delta r/r)} \tag{4}$$

So

$$\nu_{rz} = -\frac{\cos\alpha(a + l_1\cos\alpha)}{\sin\alpha(b - l_1\sin\alpha)} \tag{5}$$

In order to obtain comparison with experimental data, the variation of ν_{rz} with compressive engineering strain, ε_r^c, is required. For the translation model, the compressive engineering strain, ε_r^c, is given by

$$\varepsilon_r^c = \frac{r(\alpha) - r(\alpha = 0)}{r(\alpha = 0)} \tag{6}$$

where $r(\alpha = 0)$ is the undeformed cell size with $\alpha = 0°$ and $r(\alpha)$ is the deformed cell size with a finite angle $0 \leqslant \alpha \leqslant 90°$. This assumes that the material is in the fully expanded condition before compression testing begins and that on application of a compressive strain, the material reverts to the densified state at large strain. This assumption is borne out by SEM examinations. From equations 2 and 3

$$\varepsilon_r^c = \frac{l_1(\cos\alpha - 1)}{a + l_1} \tag{7}$$

From Equations 5 and 7, it can be seen that, at very small strains, ν_{rz} tends towards $-\infty$. As the compressive engineering strain increases, ν_{rz} becomes less negative, eventually becoming 0 at a value of strain depending on the choice of l_1.

For the rotation model, ν_{rz} can again be calculated from geometric considerations. Using a similar argument as was used from Fig. 3a now applied to Fig. 3b, gives the sides of the space-filling unit cell to be

$$r = l_2 + b\sin\Theta - a\cos\Theta \tag{8}$$

$$z = a\sin\Theta + b\cos\Theta \tag{9}$$

where Θ is the angle between the major axis of the particle and the r axis. From Equation 4, for this case

$$\nu_{rz} = \left(\frac{b\sin\Theta - a\cos\Theta}{a\sin\Theta + b\cos\Theta}\right)\left(\frac{l_2 + b\sin\Theta - a\cos\Theta}{a\sin\Theta + b\cos\Theta}\right) \tag{10}$$

The corresponding compressive engineering strain, ε_r^c, can be obtained from consideration of Equations 6 and 8 and is found to be

$$\varepsilon_r^c = \frac{b\sin\Theta - a\cos\Theta - a}{l_2 - a} \tag{11}$$

The behaviour of this model is very different to the translation model described above. Initially, a finite positive ν_{rz} is obtained which, with increasing compressive engineering strain, reaches zero and then becomes negative.

It should be noted that both these models are simplified first approximations. For a full treatment of elastic properties, it is necessary to incorporate deformable springs into the models to provide both elasticity to the system and a stable structure. However, this simple model has been very successful in predicting the full strain dependence of ν for expanded PTFE [4] indicating that the effect is dominated by the geometric arrangement of nodules and fibrils.

4. Results

4.1. Measurement of ν

Figs 4–6 plot the experimentally determined Poisson's ratio, ν_{rz}, against compressive engineering strain, ε_r^c, for the solid material extruded from the 10 mm diameter barrel (Fig. 4) and for the cup-and-cone material extruded from the 15 mm diameter barrel (Figs 5 and 6). The data used for Fig. 4 are presented in Table I, that used for Fig. 5 in Table II and that used for Fig. 6 in Table III. There are several points which should be noted. Firstly, as can be seen from the tables, results are quoted for a series of compressive tests on each specimen varying from two to five compressions. This is valid provided that the tests stay within the elastic limit of the specimens and it enables a fuller range of

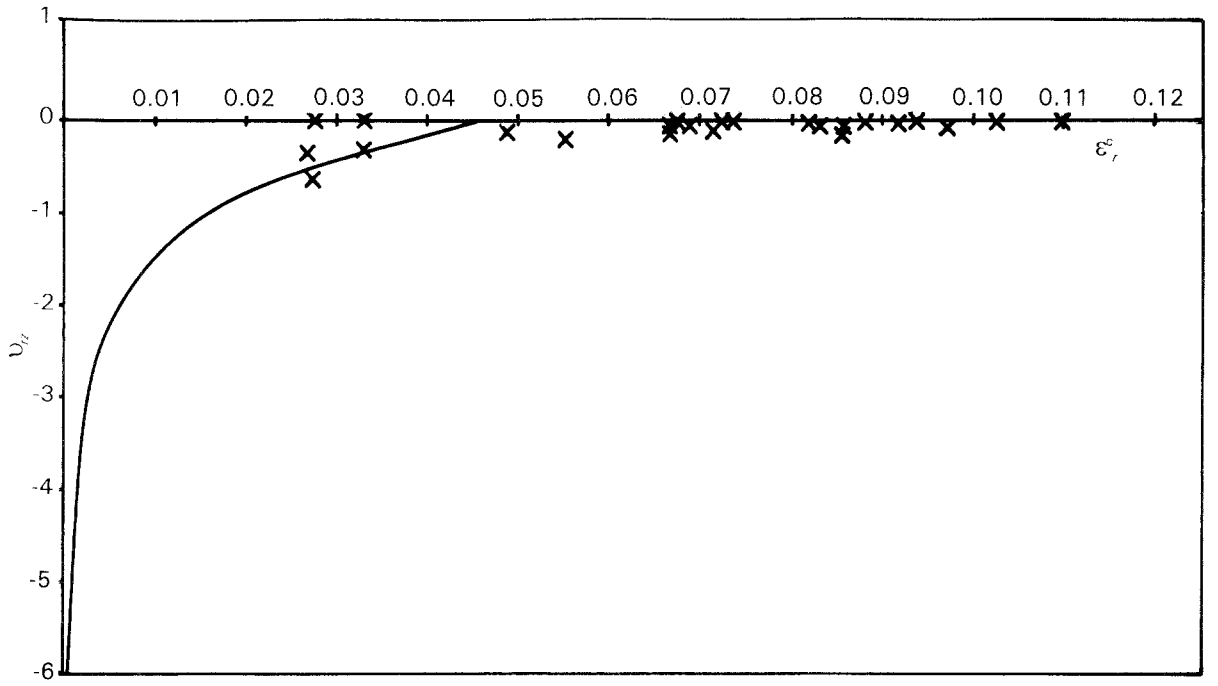

Figure 4 Plot of ν_{rz} against ε_r^c for solid material extruded from a 10 mm diameter barrel. (——) Predictions from the translation model with an aspect ratio of $a/b = 1$, (×) experimental points.

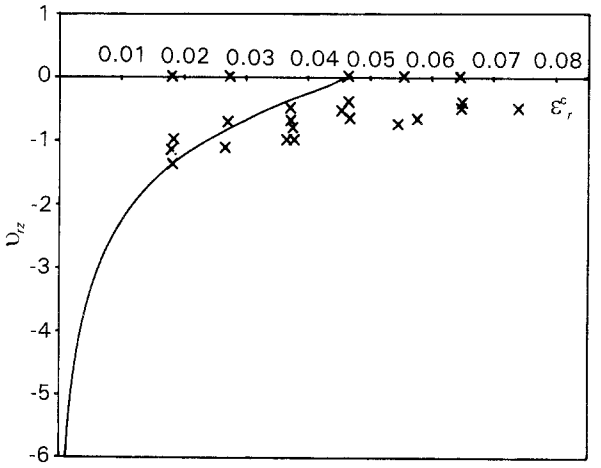

Figure 5 Plot of ν_{rz} against ε_r^c for 5 specimen sections of the cup-and-cone material extruded from a 15 mm diameter barrel. (——) Predictions from the translation model with an aspect ratio of $a/b = 1.5$, (×) experimental points.

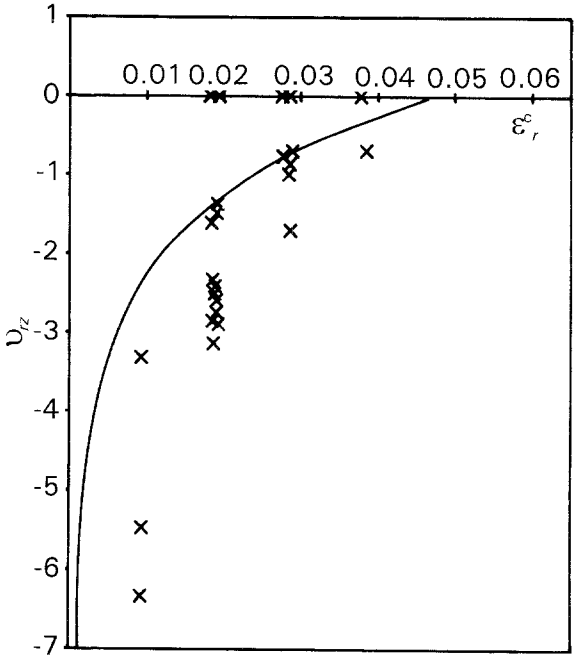

Figure 6 Plot of ν_{rz} against ε_r^c for 7 specimen sections of the cup-and-cone material extruded from a 15 mm diameter barrel. (——) Predictions from the translation model with an aspect ratio of $a/b = 1.5$, (×) experimental points.

strains to be considered for the specimens under test. It would be preferable to use one single specimen (as was done in the PTFE work [4]) and to chart its complete strain history. As already stated, however, this has not yet been possible due to problems with specimen size.

Secondly, for the solid specimens (see Table I and Fig. 4), results are plotted for 13 specimens all on the same graph. This can be done because the microstructure for the solid specimens is known to be consistent from SEM examination and, therefore, it is expected that, ideally, all specimens will behave in the same manner, producing consistent results. For the cup-and-cone specimens, however, SEM examination has revealed that the microstructure is much less consistent and thus it is necessary to plot results from separate specimens on separate graphs. Therefore, Figs 5 and 6 each plot results from a single specimen, unlike Fig. 4 where the data come from 13 separate specimens.

The final point to note is that whilst a single value of ν_{rz} was obtained for the solid specimens, ν_{rz} values for individual sections are quoted for the cup-and-cone material. This is valid because the whole cup-and-cone specimen is considered, this includes the response of a helically shaped specimen as well as the material response with the former dominating. This effect is overcome by considering the sections of the specimen individually which gives a more representative view of the material response itself.

TABLE I Engineering strain, ε_r^c and Poisson's ratio, ν_{rz} values for 13 solid specimens extruded from a 10 mm diameter barrel

Specimen	1st Compression		2nd Compression	
	ε_r^c	ν_{rz}	ε_r^c	ν_{rz}
1	0.028	0.00	0.028	0.00
2	0.056	− 0.21	0.028	− 0.64
3	0.027	− 0.36	0.068	0.00
4	0.111	0.00	0.103	0.00
5	0.111	− 0.10	0.088	0.00
6	0.097	− 0.10	0.086	− 0.17
7	0.111	0.00	0.074	0.00
8	0.071	− 0.10	0.073	0.00
9	0.049	− 0.12	0.083	− 0.07
10	0.067	− 0.09	0.033	0.00
11	0.092	− 0.05	0.094	0.00
12	0.086	− 0.07	0.069	− 0.09
13	0.067	− 0.15	0.033	− 0.33

TABLE II Engineering strain, ε_r^c and Poisson's ratio, ν_{rz}, values for 5 specimen sections extruded from a 15 mm diameter barrel

Compression	Section no.	ε_r^c	ν_{rz}
1st	1	0.065	− 0.40
	2	0.064	0.00
	3	0.055	− 0.76
	4	0.065	− 0.47
	5	0.074	− 0.51
2nd	1	0.046	− 0.53
	2	0.056	0.00
	3	0.028	− 0.74
	4	0.027	− 1.13
	5	0.038	− 1.00
3rd	1	0.037	− 0.69
	2	0.028	0.00
	3	0.027	− 0.75
	4	0.038	− 0.80
	5	0.037	− 1.02
4th	1	0.047	0.00
	2	0.047	− 0.61
	3	0.047	− 0.41
	4	0.037	− 0.49
	5	0.058	− 0.67
5th	1	0.019	0.00
	2	0.019	0.00
	3	0.019	− 1.38
	4	0.019	− 0.98
	5	0.019	− 1.10

4.2. Microscopic examination of the UHMWPE

Figs 7 and 8 are typical micrographs at magnifications of × 640 and these reveal that the microstructure for both materials is very similar and is also qualitatively similar to that seen in expanded PTFE [3]. The microstructure consists of an open network of nodules interconnected by fibrils, with the principal differences between that observed in UHMWPE and in PTFE being node shape and relative fibril length.

5. Comparison of the experimental results and the models

In order to apply the models to the experimental results for the auxetic UHMWPE material, it is necessary to measure the required parameters (i.e. a, b, l_1 and l_2) from SEM examinations of the microstructure. These measurements revealed that the average value of the particle aspect ratio was $a/b \approx 1.5$ with a large number of particles, particularly in the solid material extruded from the 10 mm diameter barrel, being circular, i.e. having an aspect ratio of $a/b \approx 1$. Thus, the aspect ratios used were $a/b = 1.5$ for the material

TABLE III Engineering strain, ε_r^c and Poisson's ratio, ν_{rz}, values for 7 specimen sections extruded from a 15 mm diameter barrel

Compression	Section no.	ε_r^c	ν_{rz}
1st	1	0.028	− 0.96
	2	0.038	0.00
	3	0.028	− 0.75
	4	0.028	0.00
	5	0.019	− 2.52
	6	0.038	0.00
	7	0.019	− 1.59
2nd	1	0.038	− 0.70
	2	0.019	− 3.12
	3	0.029	− 1.71
	4	0.019	0.00
	5	0.029	− 0.69
	6	0.019	0.00
	7	0.019	− 2.86
3rd	1	0.019	− 1.43
	2	0.019	0.00
	3	0.019	− 1.36
	4	0.009	− 5.44
	5	0.029	0.00
	6	0.000	—
	7	0.009	− 6.30
4th	1	0.019	− 1.37
	2	0.019	0.00
	3	0.029	− 0.87
	4	0.019	− 1.37
	5	0.029	0.00
	6	0.019	− 2.89
	7	0.019	− 3.12
5th	1	0.019	− 1.49
	2	0.009	− 3.31
	3	0.019	− 2.62
	4	0.019	− 2.76
	5	0.019	0.00
	6	0.019	− 1.46
	7	0.028	0.00

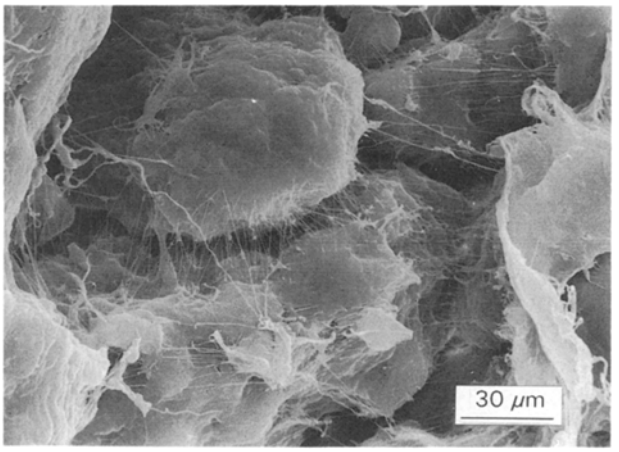

Figure 7 Micrograph of the material extruded from a barrel of diameter 15 mm.

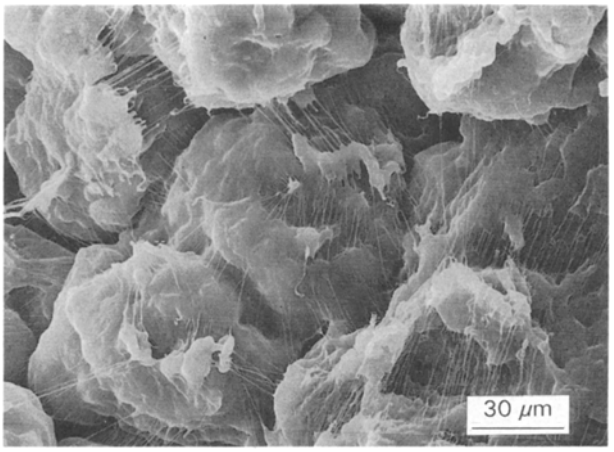

Figure 8 Micrograph of the material extruded from a barrel of diameter 10 mm.

extruded from the 15 mm diameter barrel and $a/b = 1.0$ for the material extruded from the 10 mm diameter barrel. The value of l_1 used actually determines where ν_{rz} tends to 0 and, for both aspect ratios considered, a value of $l_1 = 0.05a$ is a good approximation which is confirmed by reference to scanning electron micrographs. From Fig. 3a and b, it can be seen that l_1 and l_2 are related by

$$l_2 = 2a + l_1 \tag{12}$$

Because $l_1 = 0.05a$, then a good first approximation for l_2 is $l_2 \approx 2a$. Using these parameters, i.e. $a = b$, $l_1 = 0.05a$ and $l_2 = 2a$ for the solid material extruded from the 10 mm diameter barrel and $a = 1.5b$, $l_1 = 0.05a$ and $l_2 = 2a$ for the material extruded from the 15 mm diameter barrel, the theoretical variation of ν_{rz} with ε_r^c for both models can be obtained and plotted.

No curves for the rotational model are plotted, as it totally fails to predict the strain dependence of the material. This appears to indicate that there is no contribution to the negative ν_{rz} from particle rotation. This is not entirely surprising because, from the micrographs (Figs 7 and 8) the particles are mainly spherical with no obvious signs of twisting in the fibrillar network. It is therefore unlikely that rotation would occur.

The translation model, however, agrees very well with the experimental data, as can be seen in Figs 4–6 where the predictions from the model are plotted as solid lines. This is particularly true for Figs 4 and 5. In Fig. 6, the predictions agree well with experiment up to $\nu_{rz} = -1$. For the remainder of the results, however, although the model predicts the correct shape, ν_{rz} tends to $-\infty$ at a strain of about 0.009 and not $\varepsilon_r^c = 0$. This is probably due to the parameters a and b being slightly different in this case.

However, considering the simplicity of the translation model, very good agreement between theory and experiment has been obtained.

6. Discussion

The very good agreement between the simple translation model and experiment indicates that the mechanism for generating a negative ν_{rz} in UHMWPE is translation of the particles caused by the fibrils interconnecting them rotating during compression testing. The model uses no fitting parameters because all the geometric variables are obtained from direct SEM examination. The only other assumption (again borne out by SEM examination) is that the specimens are initially fully expanded. Unlike the expanded PTFE, it appears that there is no contribution due to the rotation of the particles. Studying the scanning electron micrographs of the UHMWPE reveals that this is no surprise (see Figs 7 and 8). Firstly, as noted previously, the aspect ratio of the particles is $a/b = 1.5$ for the cup-and-cone fractured material and $a/b = 1$ for the solid material. Because these particles are circular, or nearly circular, and no fibrillar twisting is seen, it would be expected that there is no contribution due to their rotation, unlike the PTFE case where the aspect ratio of the particles is $a/b = 5$, i.e. the particles are ellipsoid. Secondly, the PTFE microstructure was very ordered, making particle rotation a relatively easy phenomenon. In the UHMWPE, however, the microstructure is much less ordered with fibrils at several different orientations, making it very difficult for rotation of the particles to occur. Thus, the idea from the models that rotation of the particles is not part of the mechanism generating a negative ν_{rz} in UHMWPE is confirmed by microstructural analysis.

The model, as described, can only account for the observed variation of ν_{rz} as a function of strain from a consideration of the geometric constraints of the microstructure. No consideration is given to the elastic moduli of the system because the models are, as stated in Section 3, elastically unstable, providing no means for storing elastic energy. In order to incorporate this, additional features such as springs must be included [10]. This work has also shown that the fibrils are best represented by rods as opposed to strings. If the fibrils were simply inextensible strings, the model would fail because the material would not predictably collapse into a well-specified configuration. This implies that the fibrils are acting more like rods than strings to produce a well-specified condensed configuration.

Similar formulae for ν_{zr} can also be derived. The measured values of ν_{zr} are always close to zero but this may be due to the low aspect ratios of the samples preventing full contraction. This problem will not be dealt with until larger specimens are fabricated.

Taking the work on PTFE and UHMWPE together, the model has been found to work both in tension and compression. In the UHMWPE case a range of samples of different strains have been used. Hence the geometric array appears to be a stable, repeatable arrangement and, at least for UHMWPE, to be linear elastic at least for small strains. The failure of the model at higher strains may be due to inelastic or plastic behaviour of the material, with deformation of the nodules themselves or failure of the fibrils.

A further refinement to the model, apart from the inclusion of springs, would be an accurate representation of the nodules as ellipsoids. This would allow for the possibility of variations in l_1 and l_2 with angle as the fibrils wrapped around the nodules.

However, it should be noted that, despite the simplicity of the translation model used here, very good agreement with experimental data is seen.

7. Conclusion

A simple geometric model based on material microstructure has been applied to expanded UHMWPE in order to investigate the mechanisms causing the large negative Poisson's ratio seen in this material. It has been shown that the translation mechanism agrees very well with experimental data, whilst the rotation mechanism does not apply for UHMWPE. The model uses direct measurement of geometric parameters for SEM observation of the specimens and no fitting of parameters is required. The model shows that the interconnectivity of the microstructure is the principal determining factor for the measured Poisson's ratio.

Acknowledgements

The authors acknowledge the financial support of the British Technology Group. KEE acknowledges the award of an SERC Advanced Fellowship during this work.

References

1. R. S. LAKES, *Science* **235** (1987) 1038.
2. E. A. FRIIS, R. S. LAKES and J. B. PARK, *J. Mater. Sci.* **23** (1988) 4406.
3. B. D. CADDOCK and K. E. EVANS, *J. Phys. D Appl. Phys.* **22** (1989) 1877.
4. K. E. EVANS and B. D. CADDOCK, *ibid.* **22** (1989) 1883.
5. K. L. ALDERSON and K. E. EVANS, *Polymer*, **33** (1992) 4435.
6. S. HIROTSU, *J. Chem. Phys.* **94** (1991) 3949.
7. K. E. EVANS, I. J. HUTCHINSON, M. A. NKANSAH and S. C. ROGERS, *Nature* **353** (1991) 3949.
8. K. E. EVANS, *Chem. Ind.* **20** (1990) 654.
9. R. LAKES, *Dev. Mech.* **14b** (1987) 758.
10. K. E. EVANS, *J. Phys. D Appl. Phys.* **22** (1989) 1870.
11. K. E. EVANS and K. L. AINSWORTH, International Pat. WO91/01210 (1991).

Received 1 April
and accepted 17 November 1992